Modern Physics Letters B
Vol. 33, No. 0 (2021) 2150239 (10 pages)

DOI: 10.1142/S0217984921502390

Folding-mediated soft elasticity and bandgap variation in mechanical metamaterials

Guoli Wang, Ning An, Shanwen Sun and Jinxiong Zhou*

State Key Laboratory for Strength and Vibration of Mechanical Structures, School of Aerospace, Xi'an Jiaotong University, Xi'an, Shaanxi 710049, China

Shaanxi Engineering Laboratory for Vibration Control of Aerospace Structures, School of Aerospace, Xi'an Jiaotong University, Xi'an, Shaanxi 710049, China

**jxzhouxx@mail.xjtu.edu.cn*

Received 25 November 2020
Revised 29 December 2020
Accepted 14 January 2021
Published

Soft mechanical metamaterials with hinge-like elements can undergo multi-step reconfiguration through folding and contacts, and thus exhibit highly nonlinear responses. Numerical simulation of the nonlinear behaviors is essential for the design and control of the mechanical metamaterials, but it remains a challenge due to complicated nonlinear effects. Here, we report the finite element modeling of multi-step reconfiguration of a shape-changing metamaterial, and elucidate the underlying mechanism of soft elasticity. The predicted stress–strain curve together with the folding angles of hinge elements shows excellent agreement with experimental data reported in the literature. Moreover, we explore the influence of reconfiguration and folding-induced internal stress on the bandgap distribution of the mechanical metamaterials. Our efforts provide useful guidelines for the design and application of mechanical metamaterials for both static and dynamic situations.

Keywords: Mechanical metamaterials; self-folding; bandgap; soft elasticity; finite element.

1. Introduction

Mechanical metamaterials are man-made materials comprising an array of regular/irregular arrangement of unit cells, and their unusual or novel properties originate from the design and patterning of unit cells rather than from the chemistry of their constituents. Soft mechanical metamaterials are made of elastomeric materials, mainly readily fabricated via 3D printing or molding, whose behaviors are dictated by deformation, stress and motion.[1–5] Soft mechanical metamaterials have attracted increasing attentions in recent years, because of their diverse potential

applications in soft robotics,[6,7] deployable and morphing structures,[8–10] reusable energy dissipation[11–14] and flexible electronics.[15]

Soft elasticity is a notation used in the community of liquid crystal elastomers (LCEs). Soft elasticity refers to a phenomenon when a physical system undergoes a substantial deformation or an increase in strain at a fixed stress level, i.e. there exists a plateau in the stress–strain curve where the strain increases continuously while the stress remains a constant. LCE is a cross-linked polymer network entangled with rod-like liquid crystal molecules. When the alignment of these rod-like molecules is random, it is in an isotropic state; when the liquid crystal molecules align themselves along the direction, it is in a nematic state. If the LCE is deformed perpendicular to the director's direction, a soft elasticity phenomenon has been reported,[16–18] in which the LCE stretches at near-constant stress. The soft elasticity of LCE is attributed to the reorientation of the nematic director to align along the direction of the applied stretch. Reorientations of the director that are not aligned with the stretch induce continuous increase of strain while the stress remains unchanged, a highly nonlinear response observed in both experiments and simulations.[16–18]

A mechanical analogy of soft elasticity can be realized in a special class of soft mechanical metamaterials with hinge-like elements. These mechanical metamaterials include kirigami metamaterials, metamaterials with rigid parts and flexible hinge elements, etc. Under external loadings, the hinge-like elements undergo local buckling instability and the surrounding parts rotate about the hinges, resulting in continuous deformation without the need to increase the applied stress level. This type of instability-mediated soft elasticity has been demonstrated in soft mechanical metamaterials under either tension or compression.[19–23] For the tension-induced soft elasticity, it mainly occurs in some kirigami or cut-mediated metamaterials, and it is easier to simulate. For the compression-induced soft elasticity, however, it remains a challenge because the modeling involves large deformation nonlinearity, and more importantly the nonlinearity due to contacts.[21]

Very recently, shape-changing mechanical metamaterials that undergo self-guided, multi-step reconfiguration in response to global uniform compression have been demonstrated experimentally.[21] The topological reconfigurations of the mechanical metamaterial were realized by the formation of internal self-contacts between the elements of the metamaterial. A relevant multi-step deformation mechanical metamaterial was demonstrated by Meng *et al.*[24] by combining sequential snapping-through and buckling at the microscopic unit cell level. The metamaterial design by Meng *et al.*[24] is different from this study, and more importantly, the multi-step deformation was induced by uniaxial compression rather than the equi-biaxial compression considered herein. For rational design of the nonlinear mechanical elements that undergo multi-step self-guided pathways and for better understanding of the underlying nonlinear mechanics and physics, a computer modeling of the multi-step folding process is crucial for the design and control of such mechanical metamaterials. Nevertheless, it remains a blank due to the difficulties above-mentioned.

Here, we report our efforts to model the nonlinear mechanics of multi-step folding of a mechanical metamaterial under uniform compression. The numerical details of implementation in a commercial software, ABAQUS, is presented. The characteristic stress–strain curve of such a shape-changing metamaterial during a sequence of reconfigurations is successfully captured, together with the bending angles of the hinges, and good agreement is achieved between numerical simulation and experimental data reported in the literature. Our finite element modeling (FEM) data results confirm the mechanism of existence of multiple plateaus in the stress–strain curve, throwing a light on the design of mechanical metamaterials undergoing multi-step folding. Foldings, on the one hand, entail reconfiguration and shape change of the material, and, on the other hand, generate internal stress through the material. Shape change as well as the generated internal stress not only influence the quasi-static behavior of the metamaterial, but also may alter the dynamic properties of the material. We show the variation of bandgap distribution of the mechanical metamaterial due to folding, which would aid in the design of mechanical metamaterials for both static and dynamic applications, in particular, the applications focusing on vibration isolation and wave propagation.

2. Methodology

Figure 1 shows the mechanical metamaterial of interest in this paper and its dimensions. Figure 1(a) gives the metamaterial sheet with 2×2 representative volume elements (RVEs). In Ref. 21, Coulais *et al.* described in detail the material type of the finite-size metamaterial sheet (shore 80A; Silex Silicones, Ltd.), the equi-biaxial compression performed using Instron machine and the software for force–displacement data recording and processing. Our simulation accords closely with the material type and loading and boundary conditions used in the experiment by Coulais *et al.*[21] Figure 1(b) schematizes an RVE, which is comprised of a cross-shaped pattern of 20 squares and enclosed by the red square in Fig. 1(a). In Fig. 1(b), the 20 squares are classified into type 1 and type 2 according to their positions, with type 1 for central squares and type 2 for surrounding ones. Figure 1(c) shows a single square with dimensions $W \times W$ and its two hinge connections. The two hinges, one with thin width h_2, and another with thick width h_1, constitute the most flexible part and the next-most flexible part of the square, respectively. The angle α is defined as the relative rotation angle between two type-2 squares, while the angle β is defined as the rotation angle between type-1 and type-2 squares. Defined in this way, the angles α and β represent the folding angles measured at the most and the next-most flexible hinges, respectively.

The equi-biaxial compression of a 2×2 mechanical metamaterial was investigated by using ABAQUS/Explicit 2017. The 2D finite element (FE) models were constructed using plane strain approximation with the element type CPE6M, and the accuracy of the mesh was ascertained through a mesh refinement study. Two pairs of parallel plates were considered as 2D analytic rigid shells and the

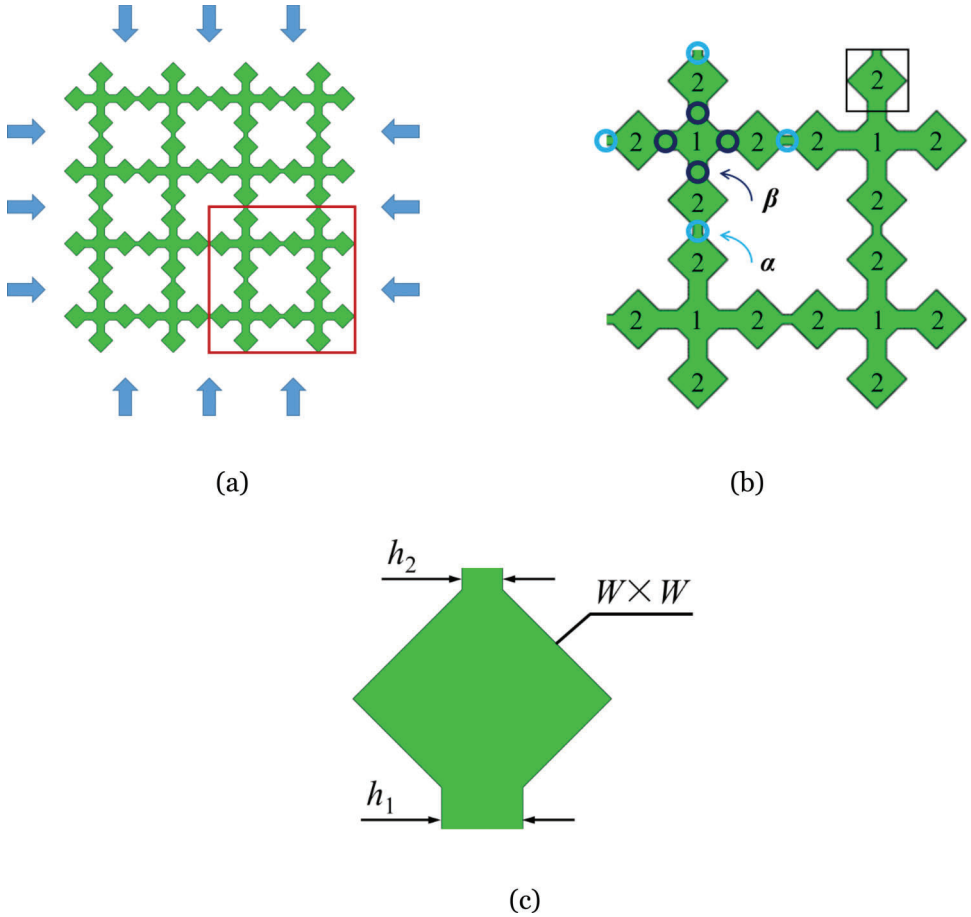

Fig. 1. (Color online) Computational model of soft mechanical metamaterial undergoing equi-biaxial compression. (a) A metamaterial with 2 × 2 RVEs being subjected to equi-biaxial compression. (b) A close-up view of the RVE enclosed by the red square in panel (a). (c) The dimensions of a unit square used to construct the metamaterial. Widths of two hinges, denoted by h_2 and h_1, are marked, corresponding to the widths of the most and the next-most flexible hinges, respectively.

loads were applied to the reference points by increasing the displacement in opposite directions to model the equi-biaxial compression of the metamaterial. Frictionless surface-to-surface contact was employed between the metamaterial and the parallel plates, while frictional self-contact was defined at internal surfaces of the metamaterial with a friction coefficient of 0.7. A small viscous pressure load was applied to damp out low-frequency dynamic effects and to attain quasi-static equilibrium with a minimal number of increments. The response of the elastomeric metamaterial was captured using a Neo-Hookean hyperelastic material model with the initial shear modulus $\mu_0 = 1$ MPa and buck modulus $K_0 = 20$ MPa $(K_0/\mu_0 = 20)$.

3. Results and Discussion

Figure 2 presents the numerical simulation results of the mechanical metamaterial in Fig. 1(a) under equi-biaxial compression. Figure 2(a) plots the stress–strain curve, where the nominal stress is normalized by the shear modulus of the material μ. The black solid line in Fig. 2(a) is the experimental result taken from the literature,[21] and the red solid line is our result from FEM. The corresponding strains and the associated deformation snapshots of the points marked by A–F in Fig. 2(a) are given in Fig. 3. Figure 2(b) plots the calculated angles, α and β, defined in Fig. 1(b), during the whole deformation process, together with the experimental measurements taken from Ref. 21. The dotted lines with markers, filled black squares and

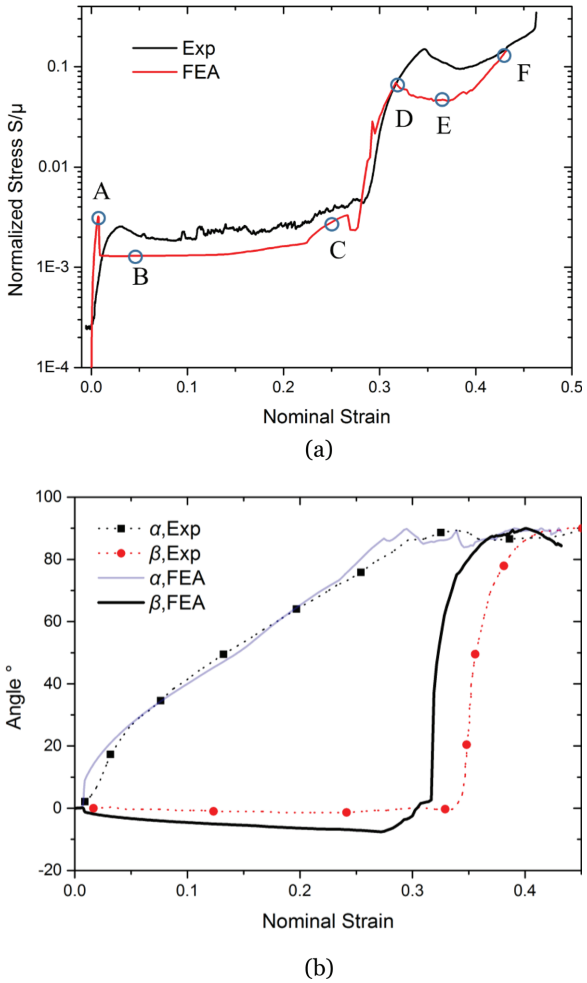

Fig. 2. (Color online) Quasi-static behavior of the finite-size mechanical metamaterial undergoing equi-biaxial compression. (a) Nominal strain versus normalized angle plot. (b) Nominal strain versus bending angle plot.

red circles, represent the experiment of α and β angles, while the solid purple line and black line represent the corresponding numerical results from FEM simulation. In Figs. 2(a) and 2(b), excellent agreement is achieved between numerical results and experiment, which verifies the correctness of our numerical scheme.

A close look at Fig. 2(a) reveals the distinct stress–strain behavior of the mechanical metamaterial undergoing multi-step folding. The material first behaves elastically until a peak of stress marked by point A is reached. A classical buckling occurs at this critical point, marked by a sharp drop of stress in numerical simulation, whereas a continuous transition occurs in experiment in this state. This is because our simulation treats ideal material and structure without imperfections, while imperfections are inevitable in the experiment. Buckling causes the most flexible hinges to bend and the rigid squares to rotate about the hinge. This rotation results in continuous increase of strain under almost a constant stress level. This gives rise to the first plateau in the stress–strain curve marked from B to C. Bending or rotating continues until the state C is attained, where self-contact occurs as shown in Fig. 3. A steep increase of applied stress is needed, as marked from C to D in Fig. 2(a), to complete the self-contact. Beyond the point D, the self-contacted rigid parts act as a single rigid part and rotate about the next-most flexible hinge as shown in Fig. 3. Then a second plateau, from D to E, forms and the plateau expands until the second self-contact begins and completes at point F. Another steep increase of stress is expected after the condensation of the whole metamaterial completes.

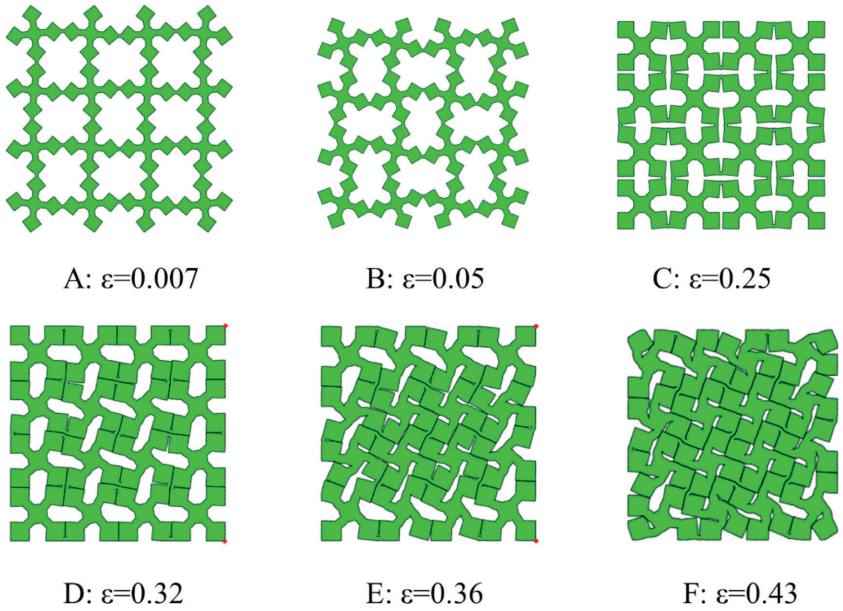

Fig. 3. (Color online) Deformation snapshots of numerical simulation of the mechanical metamaterial at various applied strains.

From our simulations presented in Figs. 2 and 3, the mechanism of self-guided, multi-step pathways of the mechanical metamaterial can be understood as follows. The central part of the square in Fig. 1(c) works as a rigid part that rotates about two hinges with different flexibilities. Upon compression, bending occurs first at the most flexible hinge, and the bending moves the rigid square until it connects with another stiff square and forms a self-contact. The connected and self-contacted rigid parts act as a single rigid part in the following deformation. If the applied compression is increased further, the second bending or rotation occurs at the next-most flexible hinge, and the bending continues until another self-contact occurs, which prevents further motion.

We then move on to study the bandgap distribution of the mechanical metamaterial, incorporating the influence of shape change and the internal stress field. The bandgap calculation chooses an RVE and enforces the Bloch boundary conditions. The details of implementation of Bloch boundary conditions in a commercial code such as ABAQUS are omitted herein and can be referred to in Ref. 25. Figure 4 presents the bandgap variations of two configurations, for both the undeformed state and deformed state, given by the left columns and right columns in Figs. 4(a) and 4(b), respectively. Figure 4(a) is for the case with $h_1 = 2$ mm and $h_2 = 1$ mm, and Fig. 4(b) is for the case with $h_1 = 1$ mm and $h_2 = 0.5$ mm, both with the same $W = 4.5$ mm. Inserted in Figs. 4(a) and 4(b) are the configurations of an RVE in the undeformed and deformed states. The deformed state was chosen as the state in the vicinity of occurrence of the first contact. To calculate the bandgap in the left column for the undeformed configurations, it is straightforward to perform a frequency analysis with Bloch boundary conditions enforced, and the bandgap calculation is performed in a single analysis step. To obtain the bandgaps in the right column in Fig. 4(b), two analysis steps are needed. Dynamic/Explicit was adopted in the first step for the quasi-static deformation process, then the linear perturbation for frequency analysis followed with the deformed configuration and internal stress from the first analysis step being retained. Note that the folding-induced variations of configuration and, in particular, the induced internal stress have profound effects on the bandgap distribution of the mechanical metamaterials. Comparing the bandgaps in Fig. 4(a), the left figure has one wide bandgap in the range of 3221–4186 Hz and one thin bandgap at around 6500 Hz. For the deformed case, the main bandgap distribution remains nearly the same as in the undeformed case. However, other additional bandgaps appear in the right column of Fig. 4(a), in particular, a very low-frequency bandgap emerges at around 300 Hz. Vibration isolation for low-frequency regime is highly desirable for various applications. These results confirm that low-frequency bandgap may be obtained by introducing shape morphing and the internal stress field. Comparison between two bandgaps in Fig. 4(b) gives similar results as in Fig. 4(a), implying that the influence of internal stress and shape variation on bandgap is a general principle. This is similar to previous study on buckling-controlled bandgap of photonic crystals.[26,27]

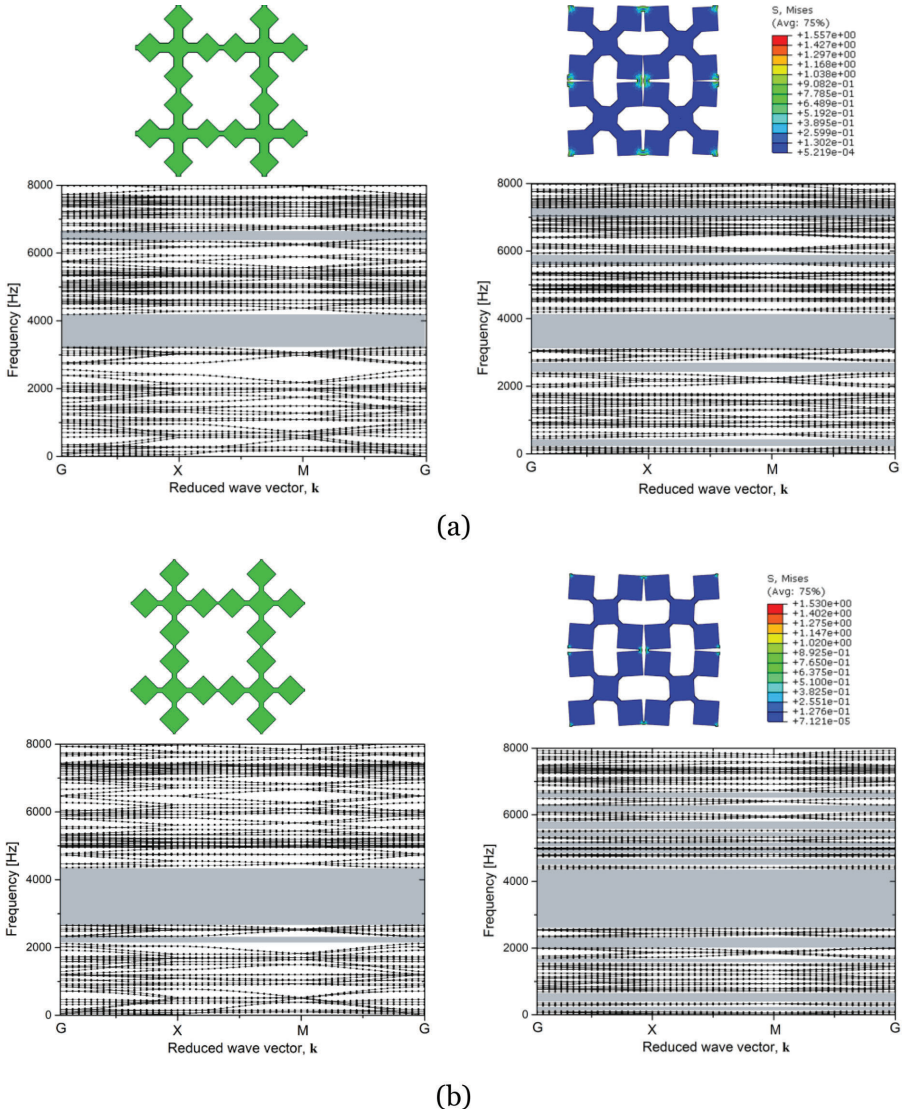

Fig. 4. (Color online) Bandgap distributions of the mechanical metamaterial with/without internal stress. Left column for the case with initial stress field. Two geometric parameters, namely, $h_1 = 2$ mm and $h_2 = 1$ mm for panel (a) and $h_1 = 1$ mm and $h_2 = 0.5$ mm for panel (b) with the same $W = 4.5$ mm, are considered.

4. Summary

We numerically investigate the quasi-static and dynamic frequency characteristics of a special soft mechanical metamaterial that can undergo self-guided multiple foldings and reconfigurations. The soft elasticity behavior of the mechanical metamaterial during equi-biaxial compression is explored. The existence of plateaus

in the stress–strain curve is captured by our simulation and good agreement is obtained between the numerical and experimental results. Folding angles are also obtained and compared well with the reported experimental data. In addition, bandgap distribution of the mechanical metamaterial is also investigated for both deformed and undeformed states. Incorporating variations of configuration and folding-induced internal stress field alters the distribution of bandgap. The emergence of a low-frequency bandgap is favored for low-frequency vibration isolation. Our efforts provide useful guidelines for the design and application of soft mechanical metamaterials.

Acknowledgments

This research is supported by Natural Science Foundation of China (Grant 11972277), and by a technological project of Institute of Systems Engineering, China Academy of Engineering Physics (2017KJZ06).

References

1. K. Bertoldi, V. Vitelli, J. Christensen and M. V. Hecke, *Nat. Rev. Mater.* **2** (2017) 17066.
2. C. Coulais, E. Teomy, K. D. Reus, Y. Shokef and M. V. Hecke, *Nature* **535** (2016) 529.
3. B. Florijn, C. Coulais and M. V. Hecke, *Phys. Rev. Lett.* **113** (2014) 175503.
4. T. Frenzel, M. Kadic and M. Wegener, *Science* **358** (2017) 1072.
5. C. Coulais, D. Sounas and A. Alã, *Nature* **542** (2017) 461.
6. A. Rafsanjani, Y. Zhang, B. Liu, S. M. Rubinstein and K. Bertoldi, *Sci. Robot.* **3** (2018) eaar7555.
7. D. Yang, B. Mosadegh, A. Ainla, B. Lee, F. Khashai, Z. Suo, K. Bertoldi and G. M. Whitesides, *Adv. Mater.* **27** (2015) 6305.
8. M. J. Mirzaali, S. Janbaz, M. Strano, L. Vergani and A. A. Zadpoor, *Sci. Rep.* **8** (2018) 965.
9. P. Celli, C. McMahan, B. Ramirez, A. Bauhofer, C. Naify, D. Hofmann, B. Audoly and C. Daraio, *Soft Matter* **14** (2018) 9744.
10. P. T. Choi, L. H. Dudte and L. Mahadevan, *Nature Mater.* **18** (2019) 999.
11. S. Shan, S. H. Kang, J. R. Raney, P. Wang, L. Fang, F. Candido, J. A. Lewis and K. Bertoldi, *Adv. Mater.* **27** (2015) 4296.
12. A. Rafsanjani, A. Akbarzadeh and D. Pasini, *Adv. Mater.* **27** (2015) 5931.
13. T. Frenzel, C. Findeisen, M. Kadic, P. Gumbsch and M. Wegener, *Adv. Mater.* **28** (2016) 5865.
14. S. Sun, N. An, G. Wang, M. Li and J. Zhou, *Appl. Phys. Lett.* **115** (2019) 091901.
15. Y. Zhang, Z. Yan, K. Nan, D. Xiao, Y. Liu, H. Luan, H. Fu, X. Wang, Q. Yang, J. Wang, W. Ren, H. Si, F. Liu, L. Yang, H. Li, J. Wang, X. Guo, H. Luo, L. Wang, Y. Huang and J. A. Rogers, *Proc. Natl. Acad. Sci. USA* **112** (2015) 11757.
16. M. Warner and E. M. Terentjev, *Liquid Crystal Elastomers* (Oxford University Press on Demand, 2003).
17. M. Warner, P. Bladon and E. M. Terentjev, *J. Phys. II (France)* **4** (1994) 93.
18. T. H. Ware, J. S. Biggins, A. F. Shick, M. Warner and T. J. White, *Nat. Commun.* **7** (2005) 10781.
19. J. N. Grima, L. Mizzi, K. M. Azzopardi and R. Gatt, *Adv. Mater.* **28** (2016) 385.

20. N. An, A. G. Domel, J. Zhou, A. Rafsanjani and K. Bertoldi, *Adv. Funct. Mater.* **30** (2020) 1906711.
21. C. Coulais, A. Sabbadini, F. Vink and M. Hecke, *Nature* **561** (2018) 512.
22. Y. Yuan, K. Zhang, B. Ratni, Q. Song, X. Ding, Q. Wu, S. N. Burokur and P. Genevet, *Nat. Commun.* **11** (2020) 4186.
23. Y. Yue, S. Sun, Y. Chen, K. Zhang, X. Ding, B. Ratni, Q. Wu, S. N. Burokur and C. Qiu, *Adv. Sci.* **7** (2020) 2001437.
24. Z. Meng, M. Liu, Y. Zhang and C. Q. Chen, *J. Mech. Phys. Solids* **144** (2020) 104095.
25. M. Åberg and P. Gudmundson, *J. Acoust. Soc. Am.* **102** (1997) 2007.
26. K. Bertoldi and M. C. Boyce, *Phys. Rev. B* **77** (2008) 052105.
27. K. Bertoldi and M. C. Boyce, *Phys. Rev. B* **78** (2008) 184107.